

Controlling the thermal conductance of silicon nitride membranes at 100 mK temperatures with patterned metal features

F

Cite as: Appl. Phys. Lett. **115**, 052601 (2019); <https://doi.org/10.1063/1.5097173>

Submitted: 22 March 2019 . Accepted: 06 July 2019 . Published Online: 02 August 2019

X. Zhang, S. M. Duff, G. C. Hilton, P. J. Lowell, K. M. Morgan , D. R. Schmidt, and J. N. Ullom

COLLECTIONS

 This paper was selected as Featured



View Online



Export Citation



CrossMark

ARTICLES YOU MAY BE INTERESTED IN

[Building ferroelectric from the bottom up: The machine learning analysis of the atomic-scale ferroelectric distortions](#)

Applied Physics Letters **115**, 052902 (2019); <https://doi.org/10.1063/1.5109520>

[Shear anisotropy-driven crystallographic orientation imaging in flexible hexagonal two-dimensional atomic crystals](#)

Applied Physics Letters **115**, 063101 (2019); <https://doi.org/10.1063/1.5096418>

[Wavelength-tunable InAsP quantum dots in InP nanowires](#)

Applied Physics Letters **115**, 053101 (2019); <https://doi.org/10.1063/1.5095675>

Lock-in Amplifiers
up to 600 MHz



Watch



Controlling the thermal conductance of silicon nitride membranes at 100 mK temperatures with patterned metal features



Cite as: Appl. Phys. Lett. **115**, 052601 (2019); doi: 10.1063/1.5097173

Submitted: 22 March 2019 · Accepted: 6 July 2019 ·

Published Online: 2 August 2019



View Online



Export Citation



CrossMark

X. Zhang,^{1,2,a)} S. M. Duff,¹ C. C. Hilton,¹ P. J. Lowell,¹ K. M. Morgan,¹  D. R. Schmidt,¹ and J. N. Ullom^{1,2}

AFFILIATIONS

¹National Institute of Standards and Technology, Boulder, Colorado 80305, USA

²Department of Physics, University of Colorado, Boulder, Colorado 80309, USA

^{a)}Electronic mail: xiaohang.zhang@colorado.edu

ABSTRACT

Freestanding micromachined membranes are often used for thermal isolation in electronic devices such as photon sensors. The degree of thermal isolation plays an important role in determining device performance, and so the ability to suppress the thermal conductance of a membrane without increasing its size or decreasing its mechanical strength is of practical importance. We present a simple method that controllably reduces the thermal conductance of silicon nitride membranes by as much as 56% at temperatures near 100 mK. The thermal conductance suppression is achieved by depositing one additional metal layer patterned into islands or rings onto the membrane surface. Complex impedance and noise measurements of superconducting transition-edge sensors fabricated using this technique show that their noise performance is not degraded.

<https://doi.org/10.1063/1.5097173>

Ultrasensitive cryogenic detectors, like superconducting Transition-Edge Sensors (TESs), operated at subkelvin temperatures are now critical to several areas of science including studies of the cosmic microwave background (CMB) which probe the structure and origins of the universe.^{1–3} Thermal sensors such as TESs require a mechanism to thermally isolate the photon absorber and thermometer element from the surrounding heat bath so that absorbed energy can be measured as a temperature change in the thermometer. The thermal isolation is often provided by freestanding, micromachined silicon or silicon nitride (SiN) membranes because the in-plane dimensions of these structures can be made much larger than their thickness. Techniques to control the thermal conductivity of freestanding membranes have obvious applications for bolometric sensors whose dynamic range, speed, physical size, and ultimate sensitivity all depend on the ease of thermal transport through the membrane.¹ For a given imaging application, there is often a thermal conductance that yields optimal performance. If the thermal conductance G falls below the optimal value, then the absorbed optical power will heat the thermometer out of its preferred temperature range, and if G exceeds the optimal value, then power fluctuations between the bath and thermometer, which grow as $G^{1/2}$, will unnecessarily degrade sensitivity.¹

When designing a freestanding membrane to achieve a target value of G , it is also necessary to consider the physical size of the structure and its mechanical robustness. Close-packed sensor arrays that

contain thousands of pixels are now expected for CMB measurements, and so matching the pixel pitch to the optical design and achieving high physical yield are required. To achieve greater thermal isolation within a finite area and to combine isolation with mechanical strength, we are exploring the impact of additional patterned features on the thermal conductivity of freestanding SiN membranes.

Considerable effort has already been devoted to controlling the thermal conductance between sensors on freestanding membranes and the surrounding thermal bath, including work to achieve higher conductances⁴ and to make the conductance more predictable.⁵ However, greater effort has been directed at achieving lower conductances for improved sensitivity. In 1995 and in subsequent work, Bock *et al.* used a silicon nitride micromesh structure to achieve low thermal conductance.^{6–8} In 1998, Holmes and colleagues reduced the thermal conductance of low stress silicon nitride membranes in several ways including patterning the membranes and gluing submicrometers sized Ag particles to the surface. The particles were the residue of an evaporated solution of ground, cured Ag epoxy, and acetone.⁹ In the same year, Leivo and Pekola also used bridge structures to lower the thermal conductance G of silicon nitride membranes.¹⁰ The use of extreme aspect ratios to reduce G continues to be explored, reaching particularly dramatic levels in the work of Beyer *et al.*¹¹ and Khosropanah *et al.*¹² Other techniques for controlling membrane G include meandering beams,¹³ trenches that do not fully perforate the

membrane,¹⁴ and metal films so thin that they form discontinuous islands.¹⁵ More recently, there has been vigorous interest in using the so-called phononic crystals in which an array of holes through a membrane or pillars on its surface modifies the phonon dispersion curves.^{16–18} Thermal transport measurements at subkelvin temperatures using these approaches are limited, although phononic crystals based on periodic hole arrays have recently been shown to suppress thermal conductance.^{19,20}

In this letter, we introduce a method to manipulate the thermal conductance G of freestanding SiN membranes without compromising the robustness of the membrane or the noise of a collocated TES sensor. We deposit and pattern an additional metal layer in different geometries on the SiN membrane. The change in G is precisely controlled by the patterning, enabling us to achieve a maximum of a 56% reduction in G . By comparing the effects of normal and superconducting metal layers, we show that phonon scattering by free electrons likely plays a role in the G suppression although we cannot rule out other mechanisms. The underlying physical principle of our technique for reducing G is thus likely the same as the Ag particles of Holmes *et al.*,⁹ but the use of modern microfabrication and patterning techniques in this work enables a far higher degree of control.

To assess the impact of metal features on phonon transport in SiN membranes, we fabricated TES thermometers with linear dimensions of $125\ \mu\text{m}$ at the center of SiN membranes with linear dimensions of $600\ \mu\text{m}$ and a thickness of $500\ \text{nm}$. The transition temperature T_c of the TESs was $90\ \text{mK}$, and the devices were cooled to temperatures from $50\ \text{mK}$ to T_c in an adiabatic demagnetization refrigerator. The TESs were operated under voltage bias, and the bias power P_b applied to the devices was equal to the power flowing through the SiN membrane to the heat bath provided by the surrounding silicon chip. It is conventional to use a power law to describe thermal transport between bodies at different temperatures, and so $P_b = \kappa(T_i^n - T_{\text{bath}}^n)$, where T_i is the internal temperature of the TES, T_{bath} is the temperature of the surrounding silicon frame, and κ and n capture the physics of phonon transport in the SiN membrane. To determine n , κ , and T_i , we acquire current-voltage curves for the TES devices at different values of T_{bath} and then extract the bias power P_b from 20% to 80% of R/R_n in increments of 10%. Values of n , κ , and T_i are determined by fitting the T_{bath} vs P_b curves at different R/R_n values with $P_b = \kappa(T_i^n - T_{\text{bath}}^n)$. Our values for n were clustered around 2.8. Knowing n , κ , and T_i , we calculated the thermal conductance G at different R/R_n using $G = dP/dT = n\kappa T_i^{n-1}$. We take the G at 80% of R/R_n as the thermal conductance for each design because the assumption that constant resistance implies constant internal temperature is most valid high in the transition where the current dependence of the resistance is small.

On some devices, a metal layer was deposited on the SiN membrane and patterned to leave features between the TES and the heat bath formed by the surrounding bulk silicon. In total, we tested 17 different designs including a control device without additional features on SiN. We measured devices where the additional metal layer was composed of $270\ \text{nm}$ of Au, a normal metal, and others where the additional layer was $54\ \text{nm}$ of Mo, a superconductor. Some of the designs with Mo were tested with duplicate devices; 23 devices were measured in total. The geometries that we tested consisted of concentric metal rings or triangular arrays of metal islands. The metal features were spaced either $7\ \mu\text{m}$ or $10\ \mu\text{m}$ apart, and the features occupied 1/3 and 2/3 of the SiN membrane, always starting at its outer perimeter.

Device geometries are shown in Fig. 1, and the measured values of G are shown in Table I.

From the G results in Table I, concentric rings or island arrays made from Mo give G reductions of 1.3%–24% compared to the control design. In contrast, concentric rings or island arrays made from Au give G reductions of 11%–56%. For identical geometries, the G reduction from Au features is substantially larger than that from Mo features. These results suggest that a normal metal is a better choice than a superconductor for reducing G although the difference in the Mo and Au thicknesses prevents a perfect comparison. We also observe that features with smaller spacing and more area coverage produce larger G reductions.

The addition of metal features to the SiN membranes creates a thermally isolated heat capacity, and so it is natural to ask if the exchange of energy between this heat capacity, the bath, and the TES is a source of unwanted thermal noise. To explore this possibility, we measured both the noise and the complex impedance of the TESs. The presence of an additional thermal body is often visible in the shape of the complex impedance curves.^{21–23} We fit the impedance data using both 1- and 2-body thermal models. We considered two 2-body models: a model in which a 2nd heat capacity dangles from the TES and a model in which a 2nd heat capacity is located between the bath and TES. We find that the complex impedance data from all devices, including the feature-free control TES, are better explained using a 2-body model. While the source of the 2nd body in the control TES is not firmly established, the observation of a 2nd thermal body even in simple structures is common.^{24,25} One possible source of additional

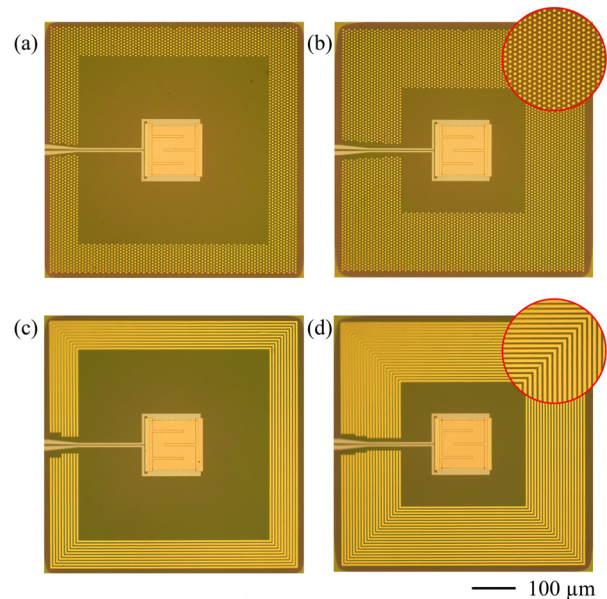


FIG. 1. Optical microscopy images of TES devices. In the pictured TESs, metal features cover 1/3 (a) and (c) and 2/3 (b) and (d) of the SiN membrane. The metal features are a triangular array of islands (a) and (b) and concentric rings (c) and (d) with a center-to-center spacing of $7\ \mu\text{m}$ ($10\ \mu\text{m}$ spacing devices are not shown in the figure). The metal islands are circular with a diameter of $4\ \mu\text{m}$, and the metal rings are $4\ \mu\text{m}$ in width. The details of the metal features can be seen in the zoomed regions of (b) and (d).

TABLE I. G of 17 designs with its standard deviation from measurements and the % reduction in G compared with the control design. 2nd body heat capacity C_2 , and calculated Au or Mo heat capacity (C_{Au} or C_{Mo}).

Spacing (μm), Metal coverage		Feature	$G \pm \sigma$ (pW/K)	Reduction %	C_2 (fJ/K)	C_{Au}, C_{Mo} (fJ/K)
N/A	N/A	N/A	111.8 ± 1.0	0	58.0	N/A
Mo	7, 2/3	Islands	91.8 ± 0.8	18	62.8	7.0×10^{-3}
Mo	7, 1/3	Islands	100.4 ± 0.9	10	70.6	3.9×10^{-3}
Mo	7, 2/3	Rings	101.2 ± 1.0	8.7	63.3	1.6×10^{-2}
Mo	7, 1/3	Rings	110.4 ± 0.9	1.5	63.4	8.8×10^{-3}
Mo	10, 2/3	Islands	84.9 ± 1.4	24	61.1	6.9×10^{-3}
Mo	10, 1/3	Islands	100.6 ± 0.8	10	59.2	3.9×10^{-3}
Mo	10, 2/3	Rings	93.2 ± 0.7	9.5	59.3	1.1×10^{-2}
Mo	10, 1/3	Rings	111.4 ± 0.8	1.3	60.6	6.1×10^{-3}
Au	7, 2/3	Islands	54.2 ± 1.1	52	62.9	103
Au	7, 1/3	Islands	82.4 ± 0.8	26	68.6	58
Au	7, 2/3	Rings	49.4 ± 1.0	56	95.9	234
Au	7, 1/3	Rings	83.7 ± 0.9	25	65.0	131
Au	10, 2/3	Islands	63.4 ± 0.8	43	72.9	102
Au	10, 1/3	Islands	99.8 ± 1.2	11	62.0	57
Au	10, 2/3	Rings	56.2 ± 0.8	50	54.2	165
Au	10, 1/3	Rings	78.9 ± 0.8	29	63.0	90

heat capacity is the amorphous SiN membrane itself.²⁶ The presence of 2-body behavior in the control TES complicates assessment of the heat capacity contribution from the additional metal features.

One candidate 2-body model for the TES is the intervening model, where the bias power in the TES passes through the 2nd thermal body. This physical picture is consistent with the bias power of the TES passing through the SiN membrane and/or the additional metal features before reaching the bath. A dangling model, where the 2nd thermal body is only coupled to the TES, and not to the bath, is also possible. The quality of impedance fits for these two models is virtually identical, as expected from Bennett *et al.*²³ Noise fitting described later in the letter supports the choice of the intervening model; noise fits with the intervening model are slightly superior to fits with the dangling model.

Fits to the complex impedance data yield numerical values for the parameters $\alpha = (T/R)(dR/dT)$ and $\beta = (I/R)(dR/dI)$ that describe the shape of the resistive transition in the TES.^{1,22} The fits also yield numerical values for the heat capacity of the 2nd thermal body C_2 , the thermal conductance $G_{\text{bath-int}}$ between the 2nd thermal body and the bath, and the thermal conductance $G_{\text{int-tes}}$ between the 2nd thermal body and the TES. To limit the number of free parameters in the fits, the heat capacity of the TES is calculated from material values and the total thermal conductance between the TES and the bath is determined from the measured TES current-voltage curves. Hence, the impedance fitting determines how the total conductance is distributed around C_2 . Values of C_2 are shown in Table I, and it can be seen that their magnitude is similar in the control TES and in devices with Mo and Au metal features. This trend suggests that the contribution of the metal features to the complex impedance is subdominant to the bare

device behavior. Table I also contains the calculated heat capacity of the superconducting Mo and normal metal Au features based on their volume and material properties. For the Au features, the estimated heat capacity is the free-electron contribution, and for the Mo features, it is the lattice contribution. The values of C_2 obtained from fitting the complex impedance cluster are around 60 fJ/K. The calculated Au values range from 57 fJ/K to 234 fJ/K depending on the volume of metal present. The similarity in these magnitudes is worth noting, but the values of C_2 extracted from the impedance fits have no obvious correlation with the volume of Au present in the different designs. The estimated heat capacities of the superconducting Mo features are far smaller than both the estimated Au values and the extracted C_2 values. C_2 values for the various G -suppressed devices are also similar to the C_2 in the bare device. The independence of the extracted C_2 values on the geometric and material details of the metal features also suggests that the contribution of the metal features to the complex impedance is subdominant to the bare device behavior.

The most definitive test of whether the additional metal features degrade device performance is through measurements of device noise such as those shown in Fig. 2. Noise spectral density is plotted vs frequency at bias fractions of 10%, 20%, and 30% of the normal state resistance for a device with normal metal features. The measurements are accompanied by theoretical predictions from the 1-body and 2-body models.²¹ For the 1-body predictions, the thermal conductance and TES resistance are obtained from the current-voltage curves of the TES, heat capacity is calculated based on the volume and the materials of the TES, α and β are obtained from fitting the complex impedance, and the excess noise M is a free parameter to be constrained by the noise data itself.²⁷ For the 2-body noise predictions, the intervening heat capacity model is used. As before, the TES heat capacity is calculated from its geometry and composition. The total thermal

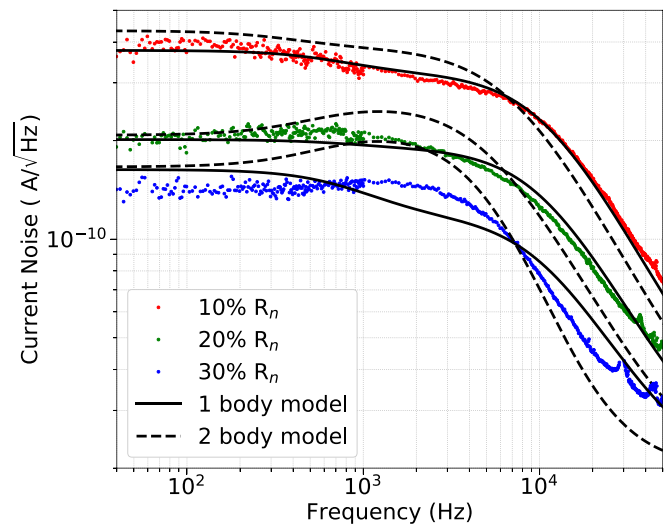


FIG. 2. Measured current noise of the TES device with Au islands with a center-to-center spacing of $7 \mu\text{m}$ and 2/3 coverage of the SiN membrane. Red, green, and blue points show the current noise of the TES biased at 10%, 20%, and 30% of R/R_n , respectively. The solid (dashed) black lines show the 1-body (2-body) model predictions for the TES noise using input parameters obtained as described in the main text.

conductance, G_{tot} and TES resistance are obtained from current-voltage curves. The complex impedance fits are used to obtain α , β , C_2 , and the ratio of the thermal conductances between C_2 and the bath and between C_2 and the TES. Like in the 1-body case, the only free parameter in the 2-body noise fits is the excess noise M .

Comparing the 1-body and 2-body noise fits among the 23 devices reveals mixed results. While the 2-body model consistently provides a superior fit to the complex impedance, the 1-body model often provides a better fit to the measured noise. In fact, the Chi-squared of the 1-body noise model is lower for 11 of the 23 devices.

Even supposing that the 2-body noise fits were unambiguously better, which they are not, their predictions at low frequencies where bolometer performance is determined are essentially equivalent to the 1-body model. Averaging over devices and multiple bias points per device, the percentage difference between the predicted and measured noise from 1 to 100 Hz was the same for the 1- and 2-body models within the margin of error. The relative success of the 1-body noise model shows that the additional metal features provide control over the device thermal conductance without introducing an unwanted noise penalty.

What microscopic picture of phonon transport explains the G suppression by metal features? There are several candidate explanations. Diffuse phonon scattering at the interface between the SiN and the metal features is possible due to differences in the density and speed of sound of the materials.²⁸ Even abrupt changes in the geometry of a uniform material can produce phonon reflection due to the different modes allowed in different volumes.^{29,30} The addition of surface features has been shown to modify phonon dispersion curves in ways that can reduce thermal conductance at low temperatures. These modifications take the form of a flattening of the dispersion curves which is associated with lower group velocities and reduced thermal conductivity.^{16,31} Finally, the absorption of phonons by free electrons in the metal features followed by thermalization and isotropic phonon re-emission is a potential source of diffuse phonon scattering in the Au but not the Mo devices.

The strong increase in G suppression from the Au features relative to the Mo features is consistent with diffuse scattering from free electrons in Au playing an important role. However, we cannot make this conclusion with complete certainty. In addition to containing unpaired electrons, the Au features are thicker than Mo (270 nm vs 54 nm) and the density and speed of sound vary between Au and Mo. As a result, Au may also have a larger effect on the phonon dispersion curves than Mo. To assess the impact of the metal features on the dispersion curves, we performed finite element method (FEM) simulations of the phonon modes using the COMSOL Multiphysics software (version 5.3a). These simulations were performed for the metal ring and island geometries with a 7 μm spacing where the effects of the added metal on G are large. The calculated dispersion curves in the presence of the Mo features were virtually unchanged from the curves for the bare devices, indicating that diffuse scattering is responsible for the G suppression in the Mo devices. However, the calculations also show nontrivial flattening of the dispersion curves in the Au devices. So even though diffuse scattering is expected to be stronger in Au than in Mo, the G suppression from the Au features may be due to a mixture of diffuse scattering and modification to the phonon dispersion curves.

Some further discussion of diffuse scattering from free electrons is warranted. In particular, we seek to answer the question of whether the normal features are likely to be strong or weak scatterers. For

strong scattering, the probability of a phonon undergoing a momentum change after encountering a metal feature is close to unity, and for weak scattering, the probability is $\ll 1$. As a thought experiment, we consider an idealized case where phonon propagation in the unpatterned membranes is fully ballistic and the normal metal features are perfect scatterers. In this case, the normal features, and especially the rings, should behave like superinsulation in a high-vacuum system. Based on work of Kropschot *et al.*,³² the first metal ring should halve the thermal conductance of the TES and N rings should reduce the conductance G_o of a bare device to $G_o/(N+1)$. However, our ring devices with the 1/3 (2/3) coverage and 7 μm spacing of the membrane have 10 (21) individual rings and the largest G reduction that we observe is about 50%. The superinsulation picture greatly overestimates the G reduction, and so one or both of the assumptions of ballistic transport and perfect scattering must be wrong. We will explore the scattering assumption followed by the ballistic transport assumption in the next two paragraphs.

The probability of a phonon interacting with the electrons of the normal metal features can be estimated using a highly simplified model. We compare the time for a phonon to transit the region of membrane underneath a metal feature to the time for a phonon to be absorbed by a free electron. The propagation time t_{transit} is given by L/v , where $L = 4 \mu\text{m}$ is a typical path length and v is the average phonon velocity at the temperature of interest. The average phonon velocity v is obtained from averaging over the derivative of the dispersion curves of Kuhn³³ to obtain the group velocity with each point weighted by the temperature-dependent Bose occupation factor. For $T = 90 \text{ mK}$, $v = 4021 \text{ m/s}$ and $t_{\text{transit}} = 1 \text{ ns}$. The characteristic time for phonon absorption by an electron in a clean metal at temperature T is given by $t_{p-e} = (234n_d k_B)/(5\Sigma T \Theta_D^3)$ using a deformation potential model in Ullom.³⁴ Here, $n_d = 5.9 \times 10^{10} \text{ atoms}/\mu\text{m}^3$ is the atomic number density of gold, k_B is the Boltzmann constant, $\Sigma = 2 \times 10^{-9} \text{ W}/(\text{K}^5 \mu\text{m}^3)$ is the electron-phonon coupling constant, and $\Theta_D = 165 \text{ K}$ is the Debye temperature. For $T = 90 \text{ mK}$, we obtain $t_{p-e} = 47 \text{ ns}$. The ratio $t_{\text{transit}}/t_{p-e} = 0.02$, which suggests that phonon scattering from single metal features is present but weak. Weak phonon scattering is consistent with the observed reductions in G being much smaller than the idealized superinsulation predictions. We caution that the specific numerical result for $t_{\text{transit}}/t_{p-e}$ should be viewed with skepticism because the expression for t_{p-e} assumed that the phonon is fully contained in the normal metal, whereas in our work, its energy is partitioned between the 500 nm thick SiN membrane and the 270 nm thick Au feature.

The assumption of ballistic transport in unpatterned membranes should also be examined. Prior measurements of mean-free-paths in SiN membranes at 100 mK yielded values in excess of 100 μm .¹⁹ Hence, we expect phonon transport in our unpatterned devices to be ballistic on length scales greater than our feature spacings. The validity of the ballistic transport assumption in our devices combined with the measured G suppressions and estimates of the phonon-electron interaction probabilities suggest weak scattering by the metal features.

In conclusion, we have demonstrated a simple method for reducing the thermal conductance of freestanding membranes without increasing their size or decreasing their mechanical strength. The thermal conductance reduction is achieved by adding additional layers of patterned metal which interfere with phonon transport; we have already achieved conductance reductions over 50% and larger

reductions are certainly possible. The noise performance of transition-edge sensors that incorporate the technique is not degraded, suggesting that this method of conductance control will have applications in the broad and growing technology area of low temperature sensors.

This work was supported by the National Aeronautics and Space Administration (NASA) Astrophysics Research and Analysis (APRA) Program. We thank Douglas Bennett, Vincent Kotsubo, John Mates, and Daniel Swetz at the National Institute of Standards and Technology for their technical assistance.

REFERENCES

- ¹K. Irwin and G. Hilton, "Transition-edge sensors," in *Cryogenic Particle Detection*, edited by C. Enss (Springer, Berlin, Heidelberg, 2005), pp. 63–150.
- ²P. A. Ade, R. W. Aikin, D. Barkats, S. J. Benton, C. A. Bischoff, J. J. Bock, J. A. Brevik, I. Buder, E. Bullock, C. D. Dowell *et al.*, "Detection of B-mode polarization at degree angular scales by BICEP2," *Phys. Rev. Lett.* **112**, 241101 (2014).
- ³R. Gualtieri, J. P. Filippini, P. A. R. Ade, M. Amiri, S. J. Benton, A. S. Bergman, R. Bihary, J. J. Bock, J. R. Bond, S. A. Bryan, H. C. Chiang, C. R. Contaldi, O. Doré, A. J. Duivenvoorden, H. K. Eriksen, M. Farhang, L. M. Fissel, A. A. Fraisse, K. Freese, M. Galloway, A. E. Gambrel, N. N. Gandilo, K. Ganga, R. V. Gramillano, J. E. Gudmundsson, M. Halpern, J. Hartley, M. Hasselfield, G. Hilton, W. Holmes, V. V. Hristov, Z. Huang, K. D. Irwin, W. C. Jones, C. L. Kuo, Z. D. Kermish, S. Li, P. V. Mason, K. Megerian, L. Moncelsi, T. A. Morford, J. M. Nagy, C. B. Netterfield, M. Nolta, B. Osherson, I. L. Padilla, B. Racine, A. S. Rahlin, C. Reintsema, J. E. Ruhl, M. C. Runyan, T. M. Ruud, J. A. Shariff, J. D. Soler, X. Song, A. Trangsud, C. Tucker, R. S. Tucker, A. D. Turner, J. F. van der List, A. C. Weber, I. K. Wehus, D. V. Wiebe, and E. Y. Young, "SPIDER: CMB polarimetry from the edge of space," *J. Low Temp. Phys.* **193**, 1112–1121 (2018).
- ⁴J. P. Hays-Wehle, D. R. Schmidt, J. N. Ullom, and D. S. Swetz, "Thermal conductance engineering for high-speed TES microcalorimeters," *J. Low Temp. Phys.* **184**, 492–497 (2016).
- ⁵K. Rostem, D. T. Chuss, F. A. Colazo, E. J. Crowe, K. L. Denis, N. P. Lourie, S. H. Moseley, T. R. Stevenson, and E. J. Wollack, "Precision control of thermal transport in cryogenic single-crystal silicon devices," *J. Appl. Phys.* **115**, 124508 (2014).
- ⁶J. Bock, D. Chen, P. Mauskopf, and A. Lange, "A novel bolometer for infrared and millimeter-wave astrophysics," *Infrared and Submillimeter Space Missions in the Coming Decade* (Springer, 1995), pp. 229–235.
- ⁷J. Bock, H. Del Castillo, A. Turner, J. Beeman, A. Lange, and P. D. Mauskopf, "Infrared bolometers with silicon nitride micromesh absorbers," in *Submillimetre and Far-Infrared Space Instrumentation* (European Space Agency, Paris, 1996), Vol. 388, p. 119.
- ⁸P. Mauskopf, J. Bock, H. Del Castillo, W. Holzappel, and A. Lange, "Composite infrared bolometers with Si₃N₄ micromesh absorbers," *Appl. Opt.* **36**, 765–771 (1997).
- ⁹W. Holmes, J. Gildemeister, P. Richards, and V. Kotsubo, "Measurements of thermal transport in low stress silicon nitride films," *Appl. Phys. Lett.* **72**, 2250–2252 (1998).
- ¹⁰M. Leivo and J. Pekola, "Thermal characteristics of silicon nitride membranes at sub-kelvin temperatures," *Appl. Phys. Lett.* **72**, 1305–1307 (1998).
- ¹¹A. Beyer, M. Kenyon, J. Bueno, P. Echternach, J. Bock, and C. Bradford, "Ultra-sensitive transition-edge sensors for far-infrared spectroscopy on SPICA," in *Twenty-First International Symposium on Space Terahertz Technology* (2010), pp. 285–290.
- ¹²P. Khosropanah, B. Dirks, M. Parra-Borderías, M. Ridder, R. Hijmering, J. van der Kuur, L. Gottardi, M. Bruijn, M. Popescu, J. Gao *et al.*, "Transition edge sensors (TES) using a low-G spider-web-like SiN supporting structure," *IEEE Trans. Appl. Supercond.* **21**, 236–240 (2011).
- ¹³M. Kenyon, P. Day, C. Bradford, J. Bock, and H. Leduc, "Background-limited membrane-isolated TES bolometers for far-IR/submillimeter direct-detection spectroscopy," *Nucl. Instrum. Methods Phys. Res. Sect., A* **559**, 456–458 (2006).
- ¹⁴V. Yefremenko, G. Wang, V. Novosad, A. Datesman, J. Pearson, R. Divan, C. Chang, T. Downes, J. McMahon, L. Bleem *et al.*, "Low temperature thermal transport in partially perforated silicon nitride membranes," *Appl. Phys. Lett.* **94**, 183504 (2009).
- ¹⁵R. Sultan, A. Avery, J. Underwood, S. Mason, D. Bassett, and B. Zink, "Heat transport by long mean free path vibrations in amorphous silicon nitride near room temperature," *Phys. Rev. B* **87**, 214305 (2013).
- ¹⁶R. Anufriev and M. Nomura, "Phonon and heat transport control using pillar-based phononic crystals," *Sci. Technol. Adv. Mater.* **19**, 863–870 (2018).
- ¹⁷B. Graczykowski, M. Sledzinska, N. Kehagias, F. Alzina, J. Reparaz, and C. Sotomayor Torres, "Hypersonic phonon propagation in one-dimensional surface phononic crystal," *Appl. Phys. Lett.* **104**, 123108 (2014).
- ¹⁸B. Graczykowski, M. Sledzinska, F. Alzina, J. Gomis-Bresco, J. Reparaz, M. Wagner, and C. S. Torres, "Phonon dispersion in hypersonic two-dimensional phononic crystal membranes," *Phys. Rev. B* **91**, 075414 (2015).
- ¹⁹N. Zen, T. A. Puurtinen, T. J. Isotalo, S. Chaudhuri, and I. J. Maasilta, "Engineering thermal conductance using a two-dimensional phononic crystal," *Nat. Commun.* **5**, 3435 (2014).
- ²⁰Y. Tian, T. A. Puurtinen, Z. Geng, and I. J. Maasilta, "Minimizing coherent thermal conductance by controlling the periodicity of two-dimensional phononic crystals," *Phys. Rev. Appl.* **12**, 014008 (2019).
- ²¹T. Miyazaki, J. N. Ullom, M. F. Cunningham, and S. E. Labov, "Noise analysis of gamma-ray TES microcalorimeters with a demonstrated energy resolution of 52 eV at 60 keV," *IEEE Trans. Appl. Supercond.* **13**, 630–633 (2003).
- ²²M. A. Lindeman, S. Bandler, R. P. Brekosky, J. A. Chervenak, E. Figueroa-Feliciano, F. M. Finkbeiner, M. J. Li, and C. A. Kilbourne, "Impedance measurements and modeling of a transition-edge-sensor calorimeter," *Rev. Sci. Instrum.* **75**, 1283–1289 (2004).
- ²³D. A. Bennett, R. D. Horansky, and J. N. Ullom, "Two-body models for analyzing complex impedance," in *AIP Conference Proceedings* (AIP, 2009), Vol. 1185, pp. 737–740.
- ²⁴B. Zink, J. Ullom, J. Beall, K. Irwin, W. Doriese, W. Duncan, L. Ferreira, G. Hilton, R. Horansky, C. Reintsema *et al.*, "Array-compatible transition-edge sensor microcalorimeter γ -ray detector with 42 eV energy resolution at 103 keV," *Appl. Phys. Lett.* **89**, 124101 (2006).
- ²⁵K. Kinnunen, "Studies of transition-edge sensor physics: Thermal models and noise," Ph.D. dissertation (University of Jyväskylä, 2011).
- ²⁶G. Wang, V. Yefremenko, V. Novosad, A. Datesman, J. Pearson, G. Shustakova, R. Divan, C. Chang, J. McMahon, L. Bleem *et al.*, "Thermal properties of silicon nitride beams below 1 kelvin," in *AIP Conference Proceedings* (AIP, 2010), Vol. 1219, pp. 75–82.
- ²⁷J. N. Ullom, W. B. Doriese, G. C. Hilton, J. A. Beall, S. Deiker, W. Duncan, L. Ferreira, K. D. Irwin, C. D. Reintsema, and L. R. Vale, "Characterization and reduction of unexplained noise in superconducting transition-edge sensors," *Appl. Phys. Lett.* **84**, 4206–4208 (2004).
- ²⁸E. T. Swartz and R. O. Pohl, "Thermal boundary resistance," *Rev. Mod. Phys.* **61**, 605–668 (1989).
- ²⁹M. Cross and R. Lifshitz, "Elastic wave transmission at an abrupt junction in a thin plate with application to heat transport and vibrations in mesoscopic systems," *Phys. Rev. B* **64**, 085324 (2001).
- ³⁰A. Beyer, M. Kenyon, B. Bumble, M. Runyan, P. Echternach, W. Holmes, J. Bock, and C. Bradford, "Comparing transition-edge sensor response times in a modified contact scheme with different support beams," *J. Low Temp. Phys.* **176**, 299–303 (2014).
- ³¹R. Anufriev and M. Nomura, "Heat conduction engineering in pillar-based phononic crystals," *Phys. Rev. B* **95**, 155432 (2017).
- ³²R. Kropschot, J. Schrodt, M. Fulk, and B. Hunter, "Multiple-layer insulation," *Advances in Cryogenic Engineering* (Springer, 1960), pp. 189–198.
- ³³T. Kühn, "Phononic transport in dielectric membranes," Ph.D. dissertation (University of Jyväskylä, 2007).
- ³⁴J. N. Ullom, "Superconducting quasiparticle behavior: Trapping, propagation, and loss," Ph.D. thesis (Harvard University, 1999).